Journal of Materials Chemistry A

ROYAL SOCIETY OF CHEMISTRY

PAPER

Cite this: J. Mater. Chem. A, 2020, 8, 11800

Nanoscale depth and lithiation dependence of V_2O_5 band structure by cathodoluminescence spectroscopy

Mitchell J. Walker, †[a] Angelique Jarry, †[b] Nick Pronin, [c] Jake Ballard, [b] Gary W. Rubloff [b] and Leonard J. Brillson *[ac]

Received 20th March 2020
Accepted 29th May 2020

DOI: 10.1039/d0ta03204b

rsc.li/materials-a

Vanadium pentoxide (V_2O_5) is a very well-known cathode material that has attracted considerable interest for its potential use in solid-state lithium-ion batteries. We pioneer the use of depth-resolved cathodoluminescence spectroscopy (DRCLS) to monitor the changes in the electronic structure of lithiated V_2O_5 from the free surface to the thin film bulk several hundred nm below as a function of lithiation. DRCLS measurements of V_2O_5 interband transitions are in excellent agreement with density functional theory (DFT) calculations. The direct measure of V_2O_5's electronic band structure as a function of lithiation level provided by DRCLS can help inform solid-state battery designs to further withstand degradation and increase efficiency. In particular, these unique electrode measurements may reveal physical mechanisms of lithiation that change V_2O_5 irreversibly, as well as methods to mitigate them in solid-state batteries.

Introduction

Research into sustainable energy technologies continues to gain importance as technologists learn more about how human activity impacts global warming and as society seeks more environmentally friendly energy sources. In line with this technological demand is the development of more efficient energy storage techniques including advanced materials for batteries. In particular, lithium-ion batteries have the potential to play a significant role in the solution of environmental problems, for example, in electric vehicles (EVs) and plug-in hybrid electric vehicles (PHEVs).[1,2] In large part, they are attractive due to their high energy density compared to other rechargeable batteries.[3]

Considerable efforts have been dedicated to developing each component of the battery system—anode materials,[4] electrolytes,[5] and cathode materials[6,7]—and to gaining a better fundamental understanding of the interfacial processes that govern the electrochemical performance of the system.[5] The thermodynamic properties of a given electrode material—in particular the reversibility of the intercalation and deintercalation reactions, the material's capability to change valence states, and the amount of available space it has to hold the ions—determine the material's lithium-ion storage capacity.[8,9] The anode materials have higher lithium-ion storage capacities than all known cathode materials.[10] Therefore, one of the primary factors to address in order to develop lithium-ion batteries with higher energy densities is the capacity of the cathode to store lithium-ions.[9]

Vanadium oxide (V_2O_5) is an interesting cathode material for lithium-ion batteries because of its high theoretical capacity of 440 mA h g^{-1} for storing three lithium ions per unit V_2O_5, or 294 mA h g^{-1} for two lithium ions per unit V_2O_5.[11] Other advantages include its low cost and easy synthesis.[12] However, several issues present challenges to its widespread use in such contexts. For example, V_2O_5's low lithium ion diffusion coefficient of 10^{-12} to 10^{-13} cm^2 s^{-1} into the matrix[13] and its moderate electrical conductivity of 10^{-2} to 10^{-3} S cm^{-1} limit its intercalation capacity and charge/discharge rate.[14,15] Another problem involves the irreversible phase transformations associated with lithiation of V_2O_5.[16–18]

The bulk structure of $Li_xV_2O_5$ with $0 < x < 3$ is well understood.[16,19–22] Pristine V_2O_5's structure consists of pyramidal VO_5 square pyramids which share edges and corners. The structure can alternatively be thought of as distorted VO_6 octahedra with perovskite-like cavities into which ions such as Li can diffuse, *i.e.*, intercalate between V_2O_5 lattice planes, making the material attractive for chemical processes involved in lithium-ion batteries. $Li_xV_2O_5$ with $x \leq 0.1$ is termed α-V_2O_5. As lithium is intercalated into the crystal structure, the layers increasingly distort or pucker. $Li_xV_2O_5$ with $0.35 \leq x \leq 0.7$ is termed ε-$Li_xV_2O_5$ and $Li_xV_2O_5$ with $0.9 \leq x \leq 1$ is termed δ-LiV_2O_5. For

[a]Department of Physics, The Ohio State University, Columbus, Ohio 43210, USA. E-mail: brillson.1@osu.edu

[b]Department of Materials Science and Engineering, Institute for Systems Research, University of Maryland, College Park, Maryland 20742, USA

[c]Department of Electrical and Computer Engineering, The Ohio State University, Columbus, Ohio, 43210 USA

† These authors contributed equally to this work.

lithiation with $x \leq 1$, the phase transitions that occur are reversible and there is little structural variation compared to pristine V_2O_5. However, upon the lithiation of more than one Li^+ per unit V_2O_5, a partially reversible phase transition to γ-$Li_xV_2O_5$ ($1 < x \leq 2$) occurs. If three Li^+ per unit V_2O_5 are intercalated, a phase termed ω-$Li_3V_2O_5$ forms. This particular phase transformation is considered irreversible as the structure does not resemble that of any other phase of $Li_xV_2O_5$, but rather that of rock salt.

V_2O_5 is also known to dissolve into liquid electrolytes during battery operation at high voltage.[23] These interfacial degradation mechanisms have a significant impact on battery performance because even a small amount of metal dissolution accompanied by surface reconstruction has a large effect over the course of many cycles.[18] The exact role of the surface chemistry, oxygen vacancy formation and surface structural rearrangement are still subject to controversies due to the complex nature of these phenomena and the inherent limitations of the standard analytical tools.[24–26]

The goal of this study is to probe how the electronic band structure of V_2O_5 changes with Li cycling as it is used as a battery cathode. We pioneer the use of depth-resolved cathodoluminescence spectroscopy (DRCLS) to monitor the changes in the V_2O_5 electronic structure as a function of lithiation and as a function of depth from the free surface to the thin film bulk several hundred nm below. The changes in the electronic band structure are measured and interpreted with reference to the reversible and irreversible structural changes that V_2O_5 undergoes over the course of lithiation to $Li_xV_2O_5$ with $0 \leq x \leq 2$.

Experimental methods

Pristine V_2O_5 samples were prepared by means of atomic layer deposition (ALD) according to Chen *et al.*'s method, using Si/SiO_2 as a substrate material.[27] A gold current-collector was deposited by DC sputtering with a thickness of 200 nm to avoid any interference of silicon peaks on the CL and Raman spectra. Fig. 1 contains illustrations of the ALD-grown V_2O_5 as well as the structural changes in the material as lithiation proceeds from α- to δ- to γ-$Li_xV_2O_5$. All V_2O_5 samples obtained through ALD have a thickness of 500 nm, with the exception of those analyzed in Fig. 3, for which the V_2O_5 layer is 200 nm thick. The film thickness was determined by contact profilometry and by scanning electron microscopy (SEM).

In order to obtain lithiated samples with approximatively one and two Li ions per unit V_2O_5, corresponding to δ-LiV_2O_5 and γ-$Li_2V_2O_5$, respectively, V_2O_5 crystalline thin films were biased in solution with V_2O_5 as the working electrode, Li foil as the counter electrode, and 1 M $LiClO_4$ dissolved in polycarbonate solvent as the electrolyte (Fig. 1). Lithium ions were intercalated into the V_2O_5 by galvanostatic cycling inside an Ar-filled glovebox using a 2 electrodes beaker cell configuration, applying a current of 8 μA (film thickness 500 nm) or 3 μA (film thickness 200 nm); the cut-off voltage dictates the lithium content and was chosen accordingly to obtain the phase of $Li_xV_2O_5$ desired: 2.8 V for δ-LiV_2O_5 and 2.2 V for γ-$Li_2V_2O_5$, as shown in Fig. 1.[19] To ensure a homogeneous repartition of the

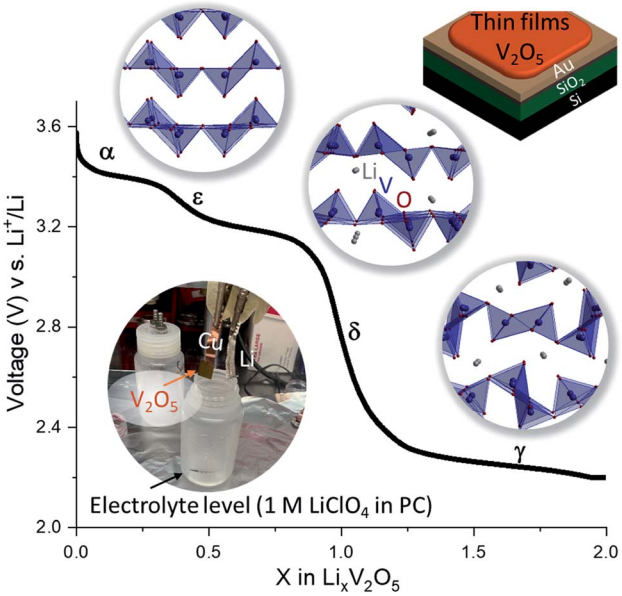

Fig. 1 The voltages applied in the beaker containing V_2O_5, Li foil, and 1 M $LiClO_4$ in PC electrolyte in order to obtain the four phases of V_2O_5 relevant to this study: α-, ε-, δ-, and γ-$Li_xV_2O_5$. In the upper-left is a picture of the sample obtained through ALD and in the lower-left, the electrochemical cell used for this study. Along the upper-right side are schematic diagrams of the structure of α-, δ-, and γ-$Li_xV_2O_5$. V atoms lie inside the nearest neighbor coordinating pyramids.

lithium within the δ-LiV_2O_5 and γ-$Li_2V_2O_5$, the voltage was maintained at the cut-off voltage until the current reached nearly zero μA, for approximatively 5 and 10 hours, respectively. For the delithiated sample, the δ-LiV_2O_5 sample was brought back to 3.4 V by galvanostatic cycling, where the voltage was maintained at this value until the current reached nearly zero μA, for approximatively 5 hours. Fig. 1 also shows images of the structure of each phase. After lithiation/delithiation, the samples underwent cleaning by means of extensive rinsing with propylene carbonate solvent inside the Ar-filled glovebox to ensure that no solid-electrolyte interface (SEI) layer was present on the surface.

Raman spectroscopy was used to probe the local structure of the samples before and after lithiation. Raman spectroscopy measurements were recorded with a confocal "Labram" microscope system (Horiba Jobin Yvon USA) equipped with a 633 nm laser source (laser power adjusted to ≤1 mW, ~2 μm beam diameter) using a 50× microscope objective (Olympus America Inc.). To maximize the spectral quality, a 600 gr mm^{-1} grating with a 30 second exposure time for 20 repetitions was used. For each composition, 2 samples and 3 different areas were measured. To prevent variations in lithium content during measurement, the samples were placed in an air-tight cell compatible with the Raman system.

Cathodoluminescence spectroscopy (CLS) provides a new and potentially useful technique to measure electronic band structure inside and at the interfaces of battery electrodes such as V_2O_5 as well many other electronic materials. This technique involves focusing an electron beam with energy of a few keV or

less onto a specimen in UHV (background pressure $\leq 2 \times 10^{-9}$ torr). This incident electron beam generates a cascade of secondary electrons with successively lower energies due to plasmon energy loss and ultimately impact ionization that results in the creation of free electron–hole (e–h) pairs.[28] These free carriers recombine either by electronic transitions between unoccupied conduction band and occupied valence band states or by transitions between defect or impurity states with levels inside the band gap and the conduction or valence band edges. These electronic transitions produce photons with energies characteristic of the material's band structure, not only the band gap between highest occupied valence and lowest unoccupied conduction band but also between higher lying unoccupied states and occupied states at the valence band maximum. These photons are collected with optical lenses, dispersed with a monochromator and the spectra recorded with a charge-coupled detector (CCD). The ability to focus the electron beam enables CLS to probe band gaps, defects, and bound states in electronic materials and devices with sub-mm to nanoscale spatial resolution and over a wider energy range of excitation than photoluminescence spectroscopy, enabling studies of higher lying conduction bands. Because the electron beam cascade extends deeper into the solid with increasing incident beam energy, one can control the depth of excitation with nanoscale precision. The CLS technique used to measure electronic properties as a function of excitation depth is termed depth-resolved CLS or DRCLS.[29] The ability of DRCLS to probe surfaces, sub-surface layers and their interfaces with nanoscale resolution can prove useful for the study of solid-state batteries, which have nanoscale lateral and depth structure whose features can provide new information about electronic and structural changes involving in battery cycling.

With increasing electron beam energy E_B, the penetration depth of the incident electron beam increases. Accordingly, cathodoluminescence spectra characteristic of the electronic band structure for E_B extending from 500 eV to 5 keV can be collected from depths of just a few nm to several hundred nm, respectively, inside the sample with depth resolution on a scale of tens of nanometers.

Fig. 2 shows penetration depths of an electron beam of a given energy in V_2O_5 calculated using Monte Carlo simulations generated by CASINO (monte CArlo SImulation of electroN trajectory in sOlids) software.[30] Besides E_B, parameters required for this simulation include density, atomic weight, and atomic number Z, of pristine V_2O_5.[31] Because the maximum beam energy used for CL in this research was 3.0 kV, penetrating ~110 nm into the sample, there is no difference in these simulations between 200 nm and 500 nm V_2O_5 layers. These simulations can be used for lithiated V_2O_5 as well, since lithiation does not significantly affect the lattice density and beam penetration depth. Each DRCLS graph is the average of five spectra, each of which consists of 10 scans, where each scan lasts 20 seconds. Spectra from several spots on each sample were tested, and several samples of each lithiation level were tested; the data presented here are therefore repeatable.

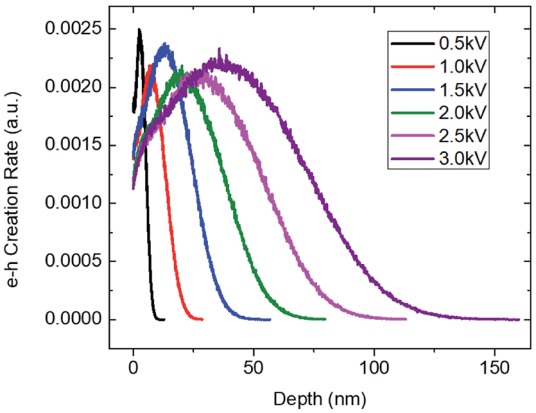

Fig. 2 Monte Carlo simulation produced with CASINO software showing the rate of e–h pair generation *versus* incident electron beam energy for α-V_2O_5.[30]

Results

We acquired DRCL spectra as a function of depth for α-, δ-, and γ-$Li_xV_2O_5$. Fig. 3a shows DRCLS on pristine (α-)V_2O_5. For E_B = 0.5 kV, which corresponds to a maximum penetration (Bohr–Bethe) range (R_B) of ~10 nm in Fig. 2, Fig. 3a shows peak features at 1.8–2, 3.2, 3.6–3.7, and 4.0 eV. When E_B is increased to 1.0 kV, corresponding to $R_B \approx 20$ nm, the broad feature around 2 eV exhibits three distinct features at 1.8, 1.9, and 2.0 eV. Higher energy features at ~3.1 eV, 3.6 eV, and 4.0 eV remain. With increasing E_B and excitation depth, the 1.8, 1.9, and 4.0 eV features increasingly dominate the spectra.

With lithiation to produce δ-LiV_2O_5 (applied voltage of 2.8 V in Fig. 1), DRCL spectra exhibit several changes. Fig. 3b shows that the features around 1.8–2.0 eV are suppressed at beam energies of 0.5 kV, although a shoulder still remains at 1.96 eV. In addition, evidence for broad emission at 2.45 eV appears with this near-surface excitation, more clearly visible in Fig. 3d. For E_B = 2.0 kV ($R_B \approx 60$ nm), all photon emissions <3 eV are suppressed. Similar to the pristine (α-V_2O_5) spectra, the 4.0 eV feature dominates at deeper beam penetration depths, but the 1.8–2.0 eV feature is absent.

With lithiation to produce γ-$Li_2V_2O_5$ (applied voltage of 2.2 V in Fig. 1), Fig. 3c shows that even the 1.96 eV feature is no longer present for any penetration depth. The weak 2.45 eV feature from δ-LiV_2O_5 in Fig. 3d remains for E_B = 0.5 kV, but is shifted to 2.5 eV. As E_B increases to 3.0 eV, this trend continues: all spectral emissions except for the 4.0 eV feature disappear. The orbital nature of all peaks in Fig. 3 and their close alignment with DFT calculations are discussed below.

DRCL spectra also provide optical information to gauge the reversibility of lithiation. Fig. 4 shows the DRCL spectra of a sample prepared as δ-LiV_2O_5 and then delithiated by galvanostatic cycling. The lithium content of the delithiated sample corresponds to ε-$Li_xV_2O_5$ with $0.1 < x < 0.3$. The 0.5 kV beam energy spectrum shows that the effects of lithiation are partially reversible. In particular, while lithiation suppressed the 1.8–2.0 eV feature, this feature returns upon delithiation, but only as

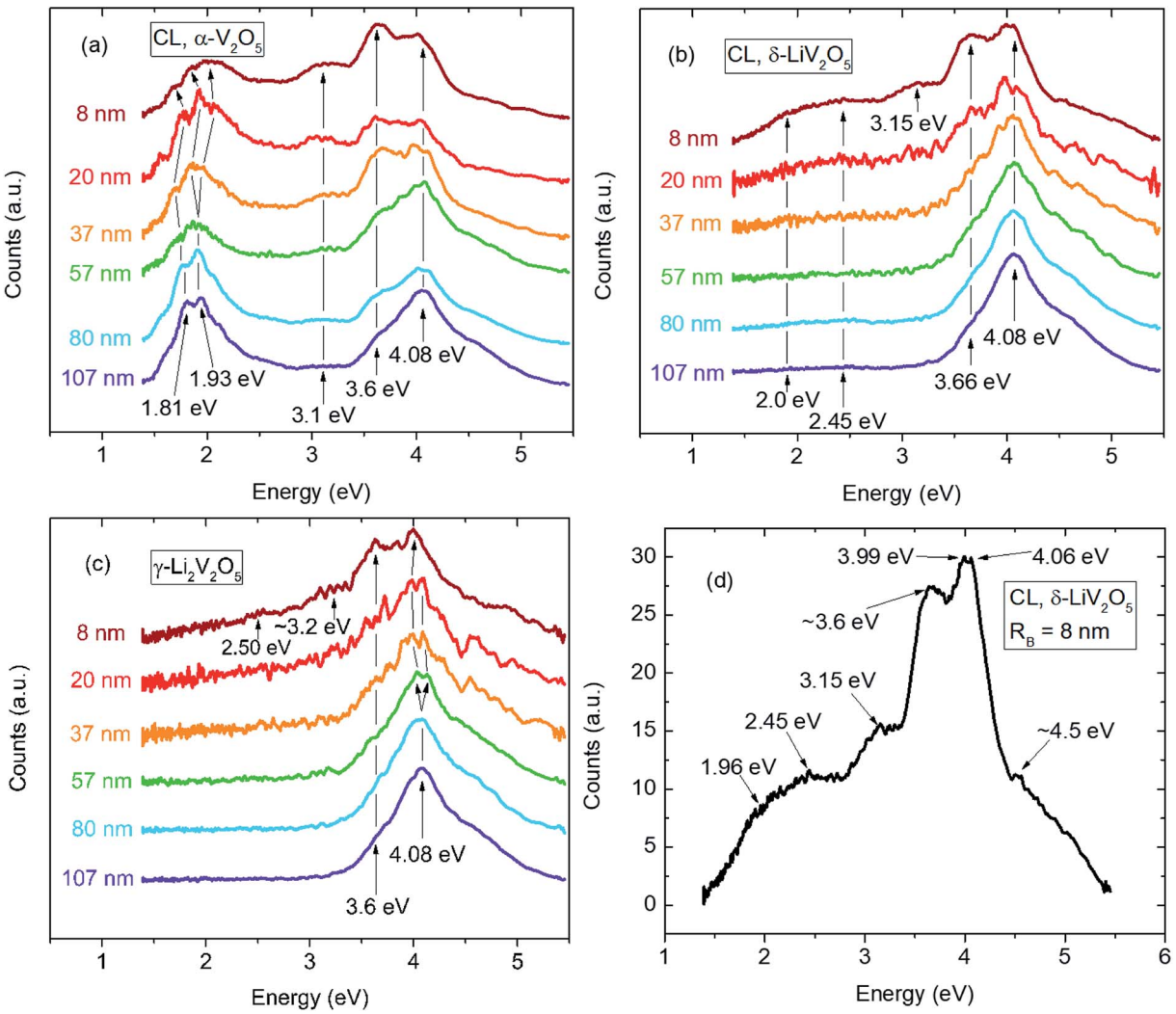

Fig. 3 CL spectra of $Li_xV_2O_5$ as a function of lithiation level ((a) $x = 0$; (b) $x = 1$; (c) $x = 2$) and incident beam energy-penetration depth. Features at 1.8, 1.9, and 4.0 eV dominate with increasing depth for pristine V_2O_5, but lithiated V_2O_5 spectra lack features around 1.8–1.9 eV, especially for R_B > 20 nm. (d) (b) near surface expanded to show 2.4 eV feature.

a very narrow peak. Even so, this relatively small feature around 1.87 eV exhibits structural broadening suggestive of the multiple peaks in that spectral region for the 1.0 kV beam energy pristine spectrum from Fig. 3a.

Even though the suppression of the 1.8–2.0 eV peaks is indeed reversible when δ-LiV_2O_5 is delithiated, the 2.45 eV feature from Fig. 3d remains at all excitation depths. In comparison, the δ-LiV_2O_5 and γ-$Li_2V_2O_5$ near-surface spectra at $E_B = 0.5$ kV in Fig. 3b and c, respectively, show that lithiation introduced a 2.45 eV feature. Since this feature is not removed when the sample is delithiated, the effects of lithiation are therefore not entirely reversible. As in all pristine and lithiated V_2O_5 spectra with $E_B = 0.5$ kV, features at ~3.7 and 4.1 eV remain as well for delithiated $Li_xV_2O_5$.

At deeper beam penetration depths, the 2.5 eV feature remains prominent, unlike in the δ-LiV_2O_5 spectrum in Fig. 3b, in which all emissions below 3 eV vanish. In addition, Fig. 4 shows a new strong 3.3 eV feature, clearly visible at $E_B = 1.0$ kV and 2.0 kV.

One physical mechanism that could change V_2O_5 with electrochemical cycling is chemical bonding between Li and O in the LiV_2O_5 scaffolds. Formation of Li–O bonds during Li intercalation could result in the formation of Li_2O and V_2O_4,[32,33] resulting in extraction of lattice oxygen from the V_2O_5 scaffold and formation of oxygen vacancies. In order to test whether such oxygen vacancies were present, we exposed both pristine and lithiated V_2O_5 to a remote oxygen plasma (ROP),[34] which has been shown to fill oxygen vacancies in ZnO,[34,35] $SrTiO_3$,[36] and Ga_2O_3.[37] Remote exposure of samples to activated oxygen in a plasma avoids lattice damage due to collisions with energetic oxygen atoms. Changes in DRCL spectra following ROP treatment might then be related to oxygen vacancies. Fig. 5a and c display the pre- and post-ROP DRCLS spectra respectively for pristine V_2O_5 with beam energies of 0.5, 2.0, and 3.0 kV. Here, ROP treatment of samples in a backfilled ultra-high vacuum chamber connected to a gas cavity linked to an RF reactor lasted for 1 hour. The pre-ROP CL spectrum in Fig. 5a appears slightly different from the pristine V_2O_5 spectrum at the same beam

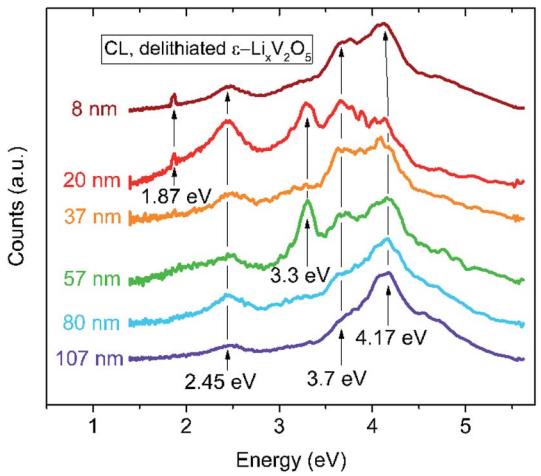

Fig. 4 DRCL spectra of delithiated $Li_xV_2O_5$ with varying beam energy and penetration depth. The features around 1.8–1.9 eV in pristine V_2O_5 spectra reappear upon delithiation, but only as a very narrow peak with a shoulder for $R_B = 8$ nm. The 2.45 eV feature visible in lithiated spectra remains for delithiated V_2O_5. A 3.3 eV feature is also visible for $E_B = 1.0$ kV and 2.0 kV in delithiated V_2O_5.

energy in Fig. 3a because it is from a different sample batch. Nevertheless, the Fig. 5a spectrum is clearly that of pristine V_2O_5.

A comparison of the pre- and post-ROP spectra shows that ROP treatment caused the V_2O_5 luminescence intensities in Fig. 5c to increase by nearly 2× for $E_B = 0.5$ kV. This is probably due to ROP cleaning the V_2O_5 surface, eliminating any adsorbates that could otherwise reduce substrate luminescence by non-radiative minority carrier recombination. Aside from this intensity difference, the ROP does not seem to have introduced, suppressed, or shifted any features in energy, confirming that the cleaning process performed with propylene carbonate removed any electrolyte residue or electrolyte surface degradation layer, *i.e.*, solid electrolyte interphases (SEI).

Fig. 5b and d show the pre- and post-ROP CL spectra for γ-$Li_2V_2O_5$. As with pristine V_2O_5, the post-ROP γ-$Li_2V_2O_5$ CL spectrum intensity for $E_B = 0.5$ kV is much higher due to ROP surface cleaning. The only difference between the pre- and post-ROP γ-$Li_2V_2O_5$ spectra is the increase in intensity of the narrow 1.88 eV peak in the post-ROP spectrum, which is very weak in the pre-ROP spectrum. Note the strong resemblance of this 1.88 eV feature with that of the delithiated V_2O_5 CL spectrum at $E_B = 0.5$ kV in Fig. 4, both of which exhibit a sharp peak with a shoulder. In general, spectra from deeper excitation depths of both pristine V_2O_5 and γ-$Li_2V_2O_5$ show no significant differences between pre- and post-ROP CL spectra. This is consistent with ROP treatment depths extending only to 50–100 nm for other semiconductors. Therefore, other than increasing near-surface CL intensity, Fig. 5 displays no significant changes with ROP treatment, implying that oxygen vacancies are not present in lithiated V_2O_5 samples.

Intercalation of lithium within α-V_2O_5 is considered to be an intercalation process. However, as discussed above, formation of Li_2O or V_2O_4 and, more generally, vanadate or oxide, during V_2O_5 battery operation, have been reported.[32,33,38] The origin of such degradation products can be potentially assigned to a conversion reaction:

$$Li_2V_2^{5+}O_5 \rightarrow Li_2O + V_2^{4+}O_4 \rightarrow Li_2O + V_2^{2+}O_3 + \tfrac{1}{2}O_{2(g)} \quad (1)$$

Alternative explanations involve lithium concentration gradients/segregation resulting in phase mixtures.[32,39,40] In order to test whether the lithiation and depth-dependent changes shown in Fig. 3–5 are due to a partial conversion reaction/lithium segregation, we took CL spectra of Li_2O powder, V_2O_3 powder, and V_2O_4 powder at $E_B = 0.5$ kV, shown in Fig. 6. Perhaps the most remarkable feature of the Li_2O spectrum (Fig. 6a) is its intensity—Li_2O luminesces at least two orders of magnitude more intensely than α, ε-, δ- or γ-$Li_xV_2O_5$. If Li_2O were present in lithiated samples in significant quantities, it would cause a substantial increase of the 2.5 and 3.1 eV features in DRCL spectra of lithiated V_2O_5 samples. There is evidence for an increase in intensity of these peaks in the delithiated V_2O_5 sample (Fig. 4), especially for $E_B = 1.0$ kV and $E_B = 2.0$ kV, for which CL spectra exhibit 2.5 eV and 3.3 eV peaks. However, whether the 3.3 eV peak visible in Fig. 4 and the 3.13 eV peak visible in Fig. 6a are the same peak is questionable. Regardless, the absence of any order-of-magnitude increase in the 2.5 eV and 3.3 eV CL peak intensities implies that Li_2O can only be present in lithiated samples in concentrations not exceeding 1%.

Conversely, V_2O_4 luminescence is significantly less than any other sample measured. The spectrum shown in Fig. 6c required 6× lower monochromator resolution to gather proportionally more light comparable or less than Fig. 6b or 3d spectra exhibit. Because of V_2O_4's exceptionally weak luminescence, even significant amounts would not contribute significantly to lithiated V_2O_5 spectra. Nevertheless, V_2O_4's peaks at ~2.0 eV and 4.05 eV bear strong resemblance to those of pristine V_2O_5 (Fig. 3a). V_2O_4 peaks at 2.5 eV and 3.22 eV resemble those of delithiated V_2O_5 (Fig. 4), and δ-LiV_2O_5 (Fig. 3b) also shares the 2.5 eV peak in common with V_2O_4, though very weakly.

As for V_2O_3 (Fig. 6b), the 2.54 eV peak and 3.18 eV peak are notable for the same reasons discussed for those peaks in V_2O_4 and Li_2O. A peak around 3.75 eV has been observed in α, ε-, δ- and γ-$Li_xV_2O_5$ spectra, and the shoulder around 2 eV is similar to those of α and δ-$Li_xV_2O_5$. Raman spectra of these various vanadium oxide phases can further refine these comparisons as discussed below.

Discussion

The optical transition energies measured by DRCLS are in excellent agreement with DFT energy bands calculated by Eyert and Höck.[41] Fig. 7a shows the partial V_{3d} t_{2g} density of states (DOS) from their work with arrows to indicate cathodoluminescence transitions from these unoccupied conduction band states to the valence band E_V maximum. This comparison of the optical emission peaks with conduction band density of states takes into account the flat V_2O_5 valence

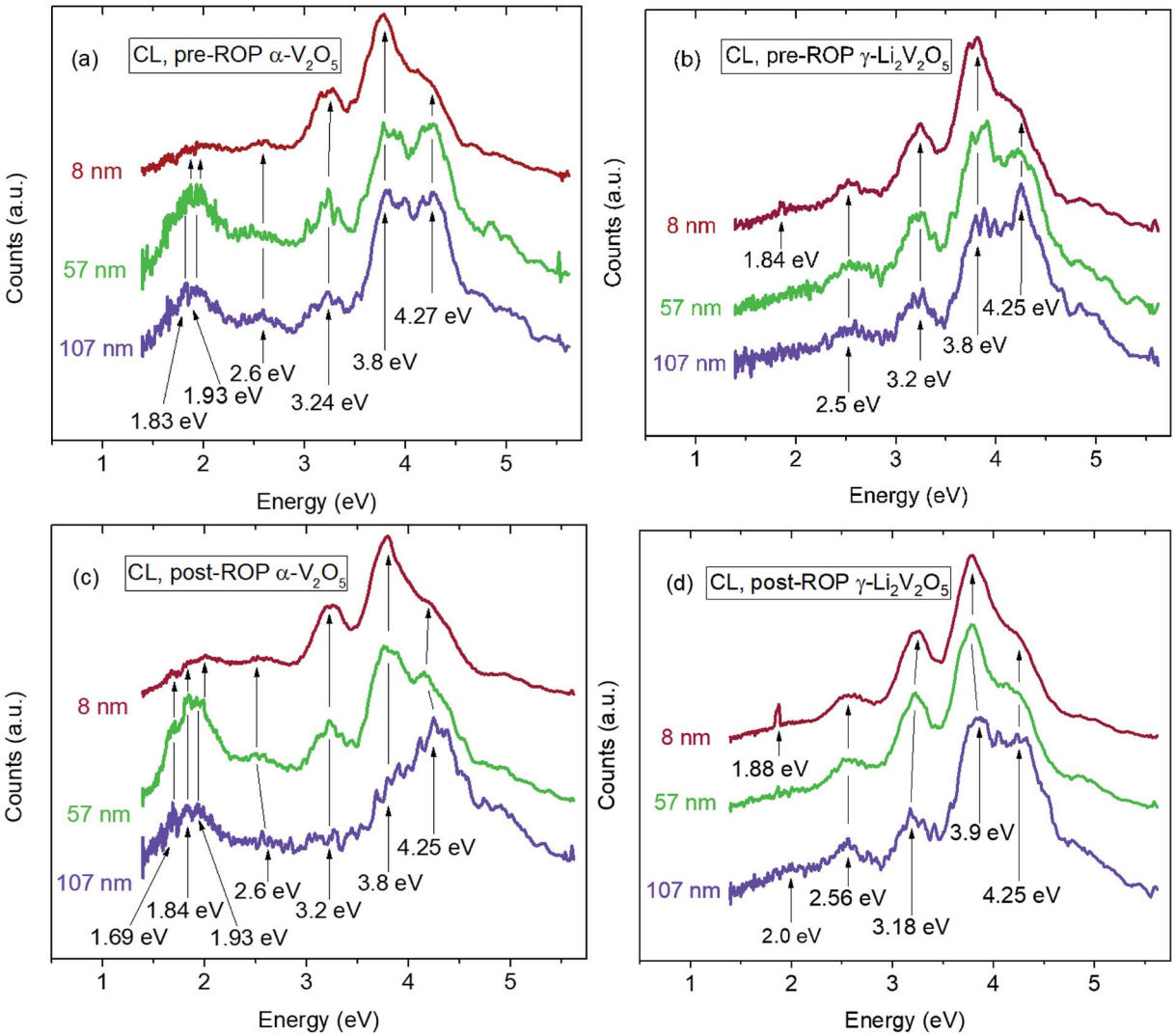

Fig. 5 DRCL spectra of (a) pristine V_2O_5 before ROP treatment, (b) γ-$Li_2V_2O_5$ before ROP treatment, (c) pristine V_2O_5 after ROP treatment, and (d) γ-$Li_2V_2O_5$ after ROP treatment, with varying beam energy and penetration depth. Other than increasing near-surface CL intensity, ROP treatment does not change the spectra significantly, implying that oxygen vacancies are not present in lithiated V_2O_5 samples.

band maximum in k-space so that direct optical transitions need not involve a joint density of states involving both valence and conduction band structure. Table 1 compares the transition energies from Fig. 7a (left column) with the DRCLS peak energies of pristine V_2O_5 from Fig. 7b (middle column). With the exception of a DFT 2.7 eV transition, weak evidence for which nevertheless appears at 2.5–2.6 eV in other α-V_2O_5 spectra, *e.g.*, Fig. 3a, the energies of all five DRCLS peaks agree with the energies of the V_{3d} t_{2g} DOS transitions to within 0.1 eV.

Based on the DFT identifications of each peak, DRCLS features can be labeled quantum mechanically with their atomic orbital character, as shown in Fig. 7b. Based on these orbital labels, the set of peaks around 1.8–2.0 eV can be attributed to a hybridization of V $3d_{xy}$–O_c $2p_x/2p_y$ states, which are based on distortions of the VO_6 octahedra. This gives rise to the split-off conduction band in the 2.1 eV range. The electrons associated with these V $3d_{xy}$–O_c $2p_x/2p_y$ states are weakly bound, so that one expects these features around 1.8–2.0 eV to be sensitive to structural distortions associated with lithiation. Indeed, these features are suppressed in δ-LiV_2O_5 spectra (Fig. 3b), and disappear completely in γ-$Li_2V_2O_5$ spectra (Fig. 3c). Furthermore, the three closely grouped features around 1.8–2.0 eV in Fig. 7b can be attributed to distortions of the VO_6 octahedra along the three crystallographic axes since the calculated partial O 2p DOS of V_2O_5 includes three closely spaced O_c $2p_x$, O_c $2p_y$, and O_c $2p_z$ peaks centered around 2 eV,[41] consistent with the orthogonal polarization dependence of three closely spaced absorption thresholds at 2.1–2.2 eV.[42] Note the very narrow 1.9 eV feature in the delithiated near-surface spectrum of Fig. 4, which may be related to one of the three VO_6 octahedra distortions resulting in square pyramids. Alternatively, the densities of states of the split-off band in both the Eyert & Höck[41] and the Bhandari *et al.*[44] densities of states exhibit just a single peak. Notwithstanding the three closely spaced and polarization-dependent absorption onsets report by Kenny *et al.*,[42] some contribution from the closely spaced

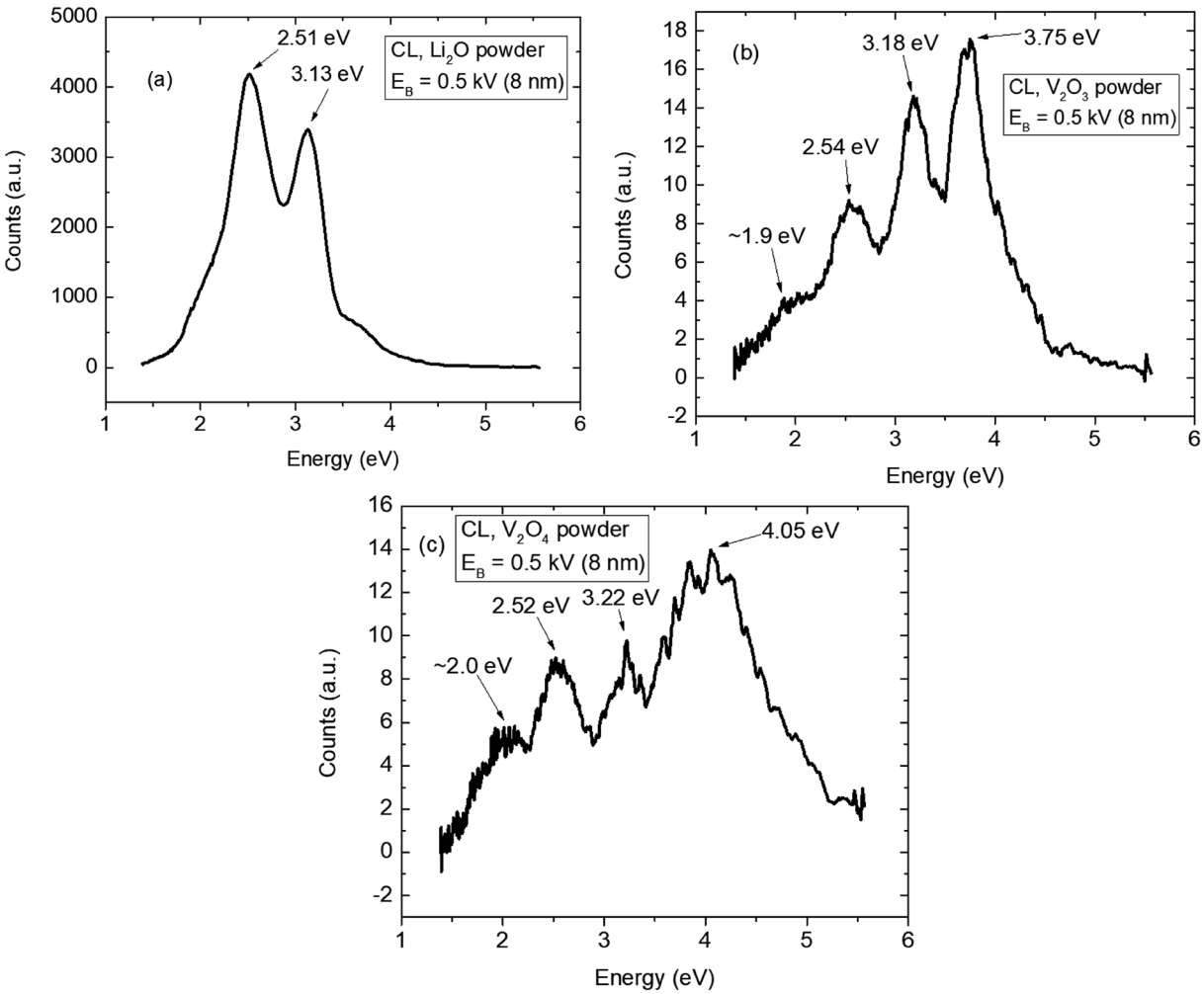

Fig. 6 DRCL spectra taken with $E_B = 0.5$ kV for (a) Li_2O powder, (b) V_2O_3 powder, and (c) V_2O_4 powder. Note the high intensity of the Li_2O CL spectrum. All peak features appear at energies present in various $Li_xV_2O_5$ CL spectra.

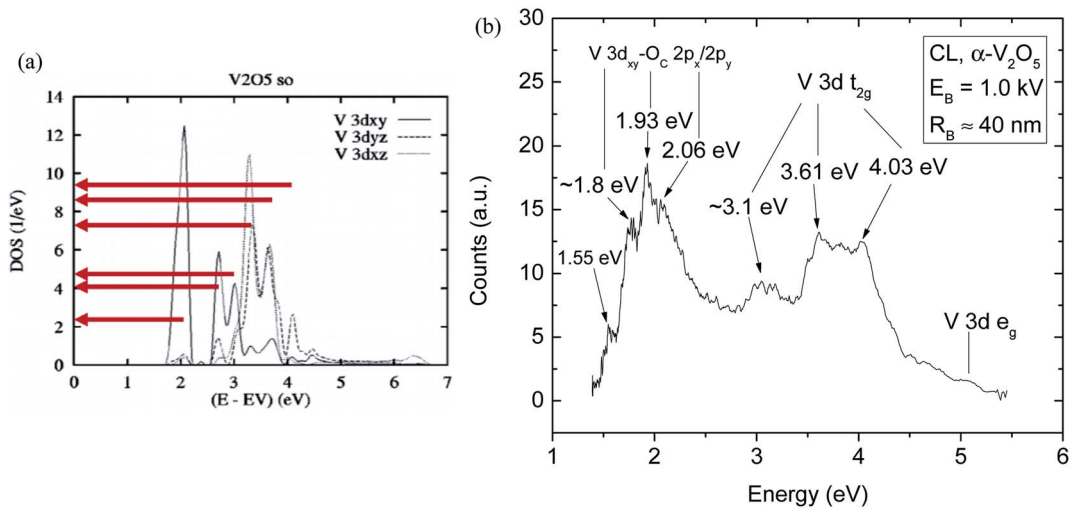

Fig. 7 (a) V_{3d} t_{2g} DOS peaks with relevant transitions[41] marked with red arrows, and (b) the pristine V_2O_5 CL spectrum with $E_B = 0.5$ kV from Fig. 3b with quantum mechanical labels based on Eyert and Höck's DFT calculations. After ref. 41 with permission, American Physical Society.

Table 1 A comparison of V_{3d} t_{2g} transitions calculated with DFT (Fig. 7a) and V_2O_5 DRCLS peaks observed in pristine V_2O_5 spectra (Fig. 7b)

V_{3d} t_{2g} DOS peaks (eV)	V_2O_5 DRCLS peaks (eV)	Interpretation (Eyert and Höck)
2.1	1.8–2	Hybridized V $3d_{xy}$–O_c $2p_x/2p_y$ states
2.7		V 3d t_{2g}
3.0	3.0	V 3d t_{2g}
3.3	3.2	V 3d t_{2g}, e_g
3.7	3.6–3.7	V 3d t_{2g}, e_g
4.1	4.0	V 3d t_{2g}

valence band splitting cannot be excluded as a possibility. DFT calculations also predict V_{3d} e_g states starting at 5–7 eV, for which Fig. 7b provides only weak evidence due to our ≤6 eV CCD detector cutoff energy.

Optical absorption measurements of Kenny *et al.* provide additional evidence for the three-fold, crystallographic nature of the split-off band.[42] Strong, fundamental absorption thresholds were reported at 2.15, 2.22, and 2.17 eV for light polarization fields E along bulk V_2O_5 crystal axes a, b, and c, respectively. Such polarization effects would not be expected for random defect distributions. Instead, defect absorption is reported at 1.24 and 1.49 eV whereas CL spectra here show no emissions at these energies. Extrapolated absorption edges exhibited direct forbidden and allowed intrinsic absorption edges between 2.35 eV and 2.45 eV, depending on crystal orientation, incident light polarization, and power law dependence modeled. Fig. 3–5 above also display 2.4–2.5 eV emissions consistent with a direct optical band gap. Hence, rather than defects, previous absorption spectra are consistent with the ~1.9–2.1 eV split-off band in addition to 2.4–2.5 eV band-to-band absorption.

The nature of the split-off band itself has been of considerable interest. Eyert and Höck attributed the split-off band to weakly bound V $3d_{xy}$–O_c $2p_x/2p_y$ derived bands that separate from the main part of unoccupied conduction band states,[41] consistent with earlier work of Lambrecht *et al.* who found the split-off bands to be related to strong indirect V–V interactions across the bridge O atoms linking the double V–O chains in the crystal structure.[43] These conduction d states correspond to the V-d orbital making the fewest antibonding interactions with O and those only with O_c-p_x but not with O-bridge p_y orbitals, that is, V_{3d} and O_{2p} orbitals with the smallest π overlap, the absence of antibonding with bridge p_y bonds,[44] and the smallest bonding–antibonding splitting.[41]

Recent works[39,45] combined DFT calculations with multimodal spectroscopies to probe the effect of lithium's presence on the α-V_2O_5 electronic structure. These studies revealed a strong impact of the lithium content on the DOS, with, from α-V_2O_5 to δ-LiV_2O_5, the reduction of the lowest split-off band V $3d_{xy}$ intensity and a shift of the t_{2g} position toward higher energies. These effects are thought to be correlated with (1) lithium segregation, (2) lattice distortion and, (3) strong hybridization of the V 3d with the O 2p.

In agreement with,[39,45] the dramatic changes in the 1.8–2.1 eV spectral regions of Fig. 3–5 with lithiation suggest that structural distortions play a major role in the degradation of V_2O_5 over the course of its use as a cathode material. This naturally leads to the question of whether lithium concentration gradients and/or a new phase of V–O–Li bonding arises with lithiation, which is associated with the band structure changes observed. In order to address this issue, we acquired Raman spectra of the pristine and lithiated V_2O_5 samples (α-, ε-, δ-, and γ-$Li_xV_2O_5$) as well as several oxides (Li_2O, V_2O_4 and V_2O_3) that could form during lithiation (Fig. 8).[32,33] Raman peak assignment for all of these compounds has been extensively discussed elsewhere.[46–51] Due to the symmetry of the system, the peaks at 995 cm^{-1} and 143 cm^{-1} of α-$Li_xV_2O_5$ are affected by the lithium intercalation more than all other peaks. The high-frequency peak at 995 cm^{-1} is associated with an out-of-plane vibration of the V_2O_5 layers: the stretching of the V=O_{apical} symmetric bond. As a consequence of lithium insertion, V=O_{apical} bonds lose their double-bond character and are elongated. This bond weakening is expected to lead to a shift toward lower frequency. On the other hand, the peak at 143 cm^{-1} is an

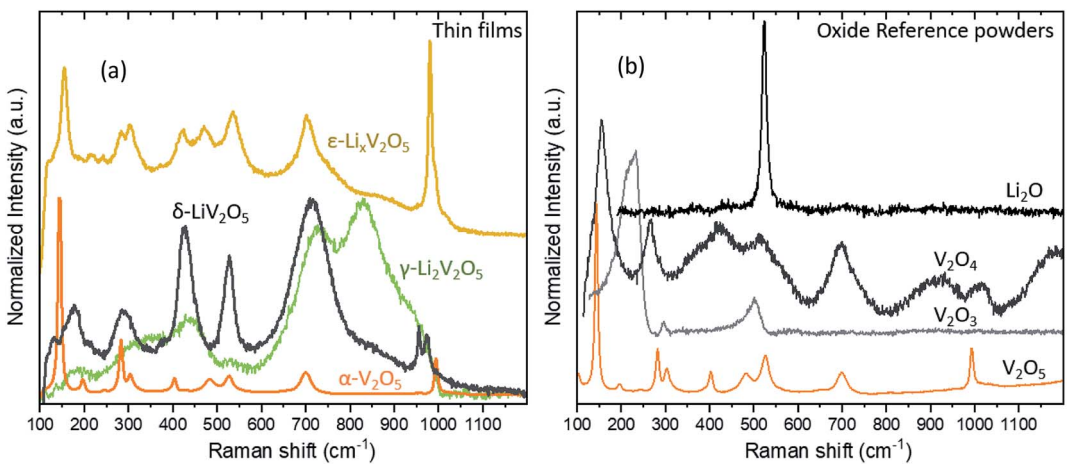

Fig. 8 (a) The Raman spectra of V_2O_5 thin film (orange) compared with that of δ-LiV_2O_5 (grey), γ-$Li_2V_2O_5$ (green), and ε-$Li_xV_2O_5$ (yellow). (b) Raman spectra of reference powders (V_2O_5, V_2O_4, V_2O_3 and Li_2O).

indicator of the in-plane order as it is related to in-phase rotation. Any increase in the amount of disorder will result in a significant shift and/or decrease of intensity of these two signature peaks. Bhandari and Lambrecht provide a more recent, full DFT description of each infrared and Raman vibrational mode.[52]

When the V_2O_5 is lithiated, Fig. 8a shows that the intensity of 143 cm^{-1} in-plane peak decreases, which is the first confirmation of the increase of disorder in the system. The out-of-plane vibration at 994 cm^{-1} shifts down with a nearly unshifted shoulder component for ε-$Li_xV_2O_5$, whereas for δ-LiV_2O_5, it splits into two peaks which shift down significantly by over 50 and 170 cm^{-1}. γ-$Li_2V_2O_5$'s peaks are shifted further down and exhibit severe broadening and splitting. The increased splitting and shifting of this out-of-plane vibrational mode are consistent with the increased out-of-plane lattice distortion and bond elongation from α- to δ- to γ-$Li_2V_2O_5$ phase transitions pictured in Fig. 1.

Next, we compared these vibrational features with those of other Li–V–O compounds to identify which are similar to those of the lithiated V_2O_5 samples (Fig. 8b). One should note that the Raman spectra of powder and film V_2O_5 are in excellent agreement (Fig. 8a and b), confirming that similar grain-size powders of the Li oxides are representative of thin films as well. V_2O_3 was eliminated as a possibility since its Raman spectra have no out-of-plane vibrational modes near 994 cm^{-1}. Indeed, V_2O_3 may not even be layered. On the other hand, Raman spectra for V_2O_4 and Li_2O bear more resemblance with those of pristine and lithiated V_2O_5. There is one Li_2O Raman frequency signature that overlaps with α-, ε-, and δ-$Li_xV_2O_5$, but not γ-$Li_2V_2O_5$, which also rules out Li_2O as a major degradation product correlated with extensive lithiation. The Raman spectrum of V_2O_4 in Fig. 8b has nearly the same in-plane mode frequencies as that of V_2O_5: a nearly unshifted 721 cm^{-1} mode, and two modes that bracket the 994 cm^{-1} modes. The origin of this similarity lies in the structure of V_2O_4, where V^{4+} is in a distorted octahedral environment of oxygen. As shown in Fig. 1, the intercalation of lithium into α-V_2O_5 is known to result in V^{5+} to V^{4+} reduction, elongation of V–O bonds, significant pyramidal chains, puckering, and rotation. Moreover, the pyramids can be described as octahedra distorted along the out-of-plane *c*-axis. The absence of the two most intense peaks at 155 and 267 cm^{-1} shows that V_2O_4 is not present as a significant phase in lithiated V_2O_5 with a quantity below the detection limits of the Raman system.

The higher degree of octahedral distortion is also consistent with the changes in DRCL spectra evident both in Fig. 3 and 4 and in Fig. 6, which shows CL spectra for Li_2O powder, V_2O_3 powder, and V_2O_4 powder at $E_B = 0.5$ kV. In agreement with their low or absent vibrational modes in the lithiated V_2O_5 Raman spectra of Fig. 8, a comparison of these spectra's features suggests that if the products of the conversion reaction Li_2O and V_2O_4 form, it would only be as minor phases, possibly as inclusions that blend at the microscale with the primary phase. Thus, we propose that the lithiation of V_2O_5 is associated with severe lattice distortion that is partially responsible for the changes in the electronic band structure observed through DRCLS and correlated with DFT-calculated energy bands. Additionally, the pre- and post-ROP CL spectra in Fig. 5 do not exhibit sub-band gap features typically observed for oxygen vacancies in oxide semiconductors,[34–37] nor does ROP remove any pre-ROP features, providing strong evidence that lithiation does not cause oxygen vacancies. In general, then, the changes in the electronic band structure reported here, visible in Fig. 3, for example, can be explained by V_2O_5 octahedral distortion rather than the formation of oxygen vacancies or secondary phases such as Li_2O and V_2O_4.

Conclusion

DRCLS measurements of $Li_xV_2O_5$'s conduction bands to valence band transitions as a function of lithiation display excellent correlation with DFT-calculated conduction energy bands. The orbital nature of these bands enables the changes in the DRCL spectra with depth and lithiation to be explained by structural distortions of the VO_6 octahedra rather than the presence of oxygen vacancies or formation of degradation products. The triplet of features around 1.8–2.0 eV corresponds to distortions of the V_2O_5's structure along its three crystallographic axes. Delithiated V_2O_5 spectra indicate that some changes associated with lithiation are reversible, whereas others are not. These changes in structure and bonding are associated with the changes in the electronic band structure detected by DRCLS. The depth-dependent electronic information presented here suggests that DRCLS can be a useful technique for probing electronic structure at V_2O_5 surfaces and buried interfaces, as well as to detect partial conversion reactions, which is of utmost importance for the rational design of lithium ion batteries and cathode materials. In turn, these measurements may improve our understanding and control of degradation processes during lithiation and battery cycling involving the electrolyte. Beyond these studies, we plan to investigate new methods of passivating the V_2O_5-electrolyte interface to minimize or prevent irreversible chemical and structural changes.

Conflicts of interest

There are no conflicts to declare.

Acknowledgements

This work was supported as part of the Nanostructures for Electrical Energy Storage (NEES), an Energy Frontier Research Center (EFRC) funded by the U.S. Department of Energy, Office of Science, Office of Basic Energy Sciences under Award Number DESC0001160 (A. J., J. B., and G. W. R.) and by the NSF grant DMR-18-00130 (M. J. W., N. P., and L. J. B.). We also acknowledge the support of the Maryland Nanocenter.

References

1 B. K. Bose, Global warming: energy, environmental pollution, and the impact of power electronics, *IEEE Ind. Electron. Mag.*, 2010, **4**, 6.

2 A. Affanni, A. Bellini, G. Franceschini, P. Guglielmi and C. Tassoni, Battery choice and management for new-generation electric vehicles, *IEEE Trans. Ind. Electron.*, 2005, **52**, 1343.

3 J.-M. Tarascon and M. Armand, Issues and challenges facing rechargeable lithium batteries, *Nature*, 2001, **414**, 359.

4 M. T. McDowell, S. W. Lee, W. D. Nix and Y. Cui, 25th anniversary article: understanding the lithiation of silicon and other alloying anodes for lithium-ion batteries, *Adv. Mater.*, 2013, **25**, 4966.

5 K. Xu, Electrolytes and interphases in Li-ion batteries and beyond, *Chem. Rev.*, 2014, **114**, 11503.

6 A. Manthiram, J. C. Knight, S. T. Myung, S. M. Oh and Y. K. Sun, "Nickel-rich and lithium-rich layered oxide cathodes: progress and perspectives, *Adv. Energy Mater.*, 2016, **6**, 1501010.

7 D. H. Seo, J. Lee, A. Urban, R. Malik, S. Kang and G. Ceder, The structural and chemical origin of the oxygen redox activity in layered and cation-disordered Li-excess cathode materials, *Nat. Chem.*, 2016, **8**, 692.

8 A. Van der Ven, J. Bhattacharya and A. A. Belak, Understanding Li diffusion in Li-intercalation compounds, *Acc. Chem. Res.*, 2012, **46**, 1216.

9 C. Liu, Z. G. Neale and G. Cao, Understanding electrochemical potentials of cathode materials in rechargeable batteries, *Mater. Today*, 2016, **19**, 109.

10 P. Liu, Vanadium-oxide-based electrode materials for Li-ion batteries, Master thesis, The University of Queensland, Australia, 2017.

11 S. Afyon, F. Krumeich, C. Mensing, A. Borgschulte and R. Nesper, New high capacity cathode materials for rechargeable Li-ion batteries: vanadate-borate glasses, *Sci. Rep.*, 2014, **4**, 7113.

12 Y. Wang and G. Cao, Developments in nanostructured cathode materials for high-performance lithium-ion batteries, *Adv. Mater.*, 2008, **20**, 2251.

13 F. Lantelme, A. Mantoux, H. Groult and D. Lincot, Electrochemical study of phase transition processes in lithium insertion in V_2O_5 electrodes, *J. Electrochem. Soc.*, 2003, **150**, A1202.

14 F. Coustier, J. Hill, B. B. Owens, S. Passerini and W. H. Smyrl, Doped vanadium oxides as host materials for lithium intercalation, *J. Electrochem. Soc.*, 1999, **146**, 1335.

15 J. Livage, Vanadium pentoxide gels, *Chem. Mater.*, 1991, **3**, 578.

16 X. Li, W. Li, H. Ma and J. Chen, Electrochemical lithium intercalation/deintercalation of single-crystalline V_2O_5 nanowires, *J. Electrochem. Soc.*, 2007, **154**, A39.

17 J. M. Cocciantelli, J. P. Doumerc, M. Pouchard, M. Broussely and J. Labat, Crystal chemistry of electrochemically inserted $Li_xV_2O_5$, *J. Power Sources*, 1991, **34**, 103.

18 M. Winter, J. O. Besenhard, M. E. Spahr and P. Novák, Insertion electrode materials for rechargeable lithium batteries, *Adv. Mater.*, 1998, **10**, 725.

19 C. Delmas, H. Cognac-Auradou, J. M. Cocciantelli, M. Ménétrier and J. P. Doumerc, The $Li_xV_2O_5$ system: an overview of the structure modifications induced by the lithium intercalation, *Solid State Ionics*, 1994, **69**, 257.

20 J. S. Braithwaite, C. R. A. Catlow, J. D. Gale and J. H. Harding, Lithium intercalation into vanadium pentoxide: a theoretical study, *Chem. Mater.*, 1999, **11**, 1990.

21 Y. Yue and H. Liang, Micro-and nano-structured vanadium pentoxide (V_2O_5) for electrodes of lithium-ion batteries, *Adv. Energy Mater.*, 2017, **7**, 1602545.

22 X. Rocquefelte, F. Boucher, P. Gressier and G. Ouvrard, First-principle study of the intercalation process in the $Li_xV_2O_5$ system, *Chem. Mater.*, 2003, **15**, 1812.

23 Q. Qu, Y. Zhu, X. Gao and Y. Wu, "Core–shell structure of polypyrrole grown on V_2O_5 nanoribbon as high performance anode material for supercapacitors, *Adv. Energy Mater.*, 2012, **2**, 950.

24 X. Gao, Y. H. Ikuhara, C. A. J. Fisher, R. Huang, A. Kuwabara, H. Moriwake, K. Kohama and Y. Ikuhara, Oxygen loss and surface degradation during electrochemical cycling of lithium-ion battery cathode material $LiMn_2O_4$, *J. Mater. Chem. A*, 2019, **7**, 8845.

25 D. Qian, B. Xu, M. Chi and Y. S. Meng, Uncovering the roles of oxygen vacancies in cation migration in lithium excess layered oxides, *Phys. Chem. Chem. Phys.*, 2014, **16**, 14665.

26 A. Jarry, S. Gottis, Y. S. Yu, J. Roque-Rosell, C. Kim, J. Cabana, J. Kerr and R. Kostecki, "The formation mechanism of fluorescent metal complexes at the $Li_xNi_{0.5}Mn_{1.5}O_{4-\delta}$/carbonate ester electrolyte interface, *J. Am. Chem. Soc.*, 2015, **137**, 3533.

27 X. Chen, E. Pomerantseva, P. Banerjee, K. Gregorczyk, R. Ghodssi and G. Rubloff, Ozone-based atomic layer deposition of crystalline V_2O_5 films for high performance electrochemical energy storage, *Chem. Mater.*, 2012, **24**, 1255.

28 A. Rose, Energy Losses by Hot Electrons, *RCA Rev.*, 1966, **27**, 600.

29 L. J. Brillson, Applications of Depth-Resolved Cathodoluminescence Spectroscopy, *J. Phys. D: Appl. Phys.*, 2012, **45**, 183001.

30 D. Drouin, A. R. Couture, D. Joly, X. Tastet, V. Aimez and R. Gauvin, CASINO V2. 42—a fast and easy-to-use modeling tool for scanning electron microscopy and microanalysis users, *Scanning*, 2007, **29**, 92.

31 L. J. Brillson, in *Surfaces and Interfaces of Electronic Materials*, John Wiley & Sons, Weinheim, Germany, 2010, ch. 16.

32 A. Mukherjee, H. A. Ardakani, T. Yi, J. Cabana, R. Shahbazian-Yassar and R. F. Klie, Direct characterization of the Li intercalation mechanism into α-V_2O_5 nanowires using in situ transmission electron microscopy, *Appl. Phys. Lett.*, 2017, **110**, 213903.

33 K. J. Rao, B. Pecquenard, A. Gies, A. Levasseur and J. Etourneau, Structural and electrochemical behaviour of sputtered vanadium oxide films: oxygen non-stoichiometry and lithium ion sequestration, *Bull. Mater. Sci.*, 2006, **29**, 535.

34 H. L. Mosbacker, Y. M. Strzhemechny, B. D. White, P. E. Smith, D. C. Look, D. C. Reynolds, C. W. Litton and L. J. Brillson, Role of near-surface states in ohmic-Schottky

conversion of Au contacts to ZnO, *Appl. Phys. Lett.*, 2005, **87**, 012102.
35 Y. Dong, Z. Q. Fang, B. Claflin, D. C. Look, Y. F. Dong and L. J. Brillson, Metal contacts on bulk ZnO crystal treated with remote oxygen plasma, *J. Vac. Sci. Technol., B: Microelectron. Nanometer Struct.–Process., Meas., Phenom.*, 2009, **27**, 1774.
36 M. M. Rutkowski, K. McNicholas, Z. Q. Zeng, F. Tuomisto and L. J. Brillson, Optical identification of oxygen vacancy formation at $SrTiO_3$-(Ba,Sr)TiO_3 heterostructures, *J. Phys. D: Appl. Phys.*, 2014, **47**, 255303.
37 H. Gao, S. Muralidharan, N. Pronin, Md. R. Karim, S. M. White, T. Asel, G. Foster, S. Krishnamoorthy, S. Rajan, L. R. Cao, M. Higashiwaki, H. von Wenckstern, M. Grundmann, H. Zhao, D. C. Look and L. J. Brillson, Optical signatures of deep level defects in Ga_2O_3, *Appl. Phys. Lett.*, 2018, **112**, 242102.
38 P. M. Marley, G. A. Horrocks, K. E. Pelcher and S. Banerjee, Transformers: the changing phases of low-dimensional vanadium oxide bronzes, *Chem. Commun.*, 2015, **51**, 5181.
39 G. A. Horrocks, E. J. Braham, Y. Liang, L. R. De Jesus, J. Jude, J. M. Velázquez, D. Prendergast and S. Banerjee, Vanadium k-edge x-ray absorption spectroscopy as a probe of the heterogeneous lithiation of V_2O_5: first-principles modeling and principal component analysis, *J. Phys. Chem. C*, 2016, **120**, 23922.
40 C. K. Chan, H. Peng, R. D. Twesten, K. Jarausch, X. F. Zhang and Y. Cui, Fast, completely reversible Li insertion in vanadium pentoxide nanoribbons, *Nano Lett.*, 2007, **7**, 490.
41 V. Eyert and K. H. Höck, Electronic structure of V_2O_5: role of octahedral deformations, *Phys. Rev. B: Condens. Matter Mater. Phys.*, 1998, **57**, 12727.
42 N. Kenny, C. R. Kannewurf and D. H. Whitmore, Optical absorption coefficients of vanadium pentoxide single crystals, *J. Phys. Chem. Solids*, 1966, **27**, 1237.
43 W. Lambrecht, B. Djafari-Rouhani and J. Vennik, On the origin of the split-off conduction bands in V_2O_5, *J. Phys. C: Solid State Phys.*, 1981, **14**, 4785.
44 C. Bhandari, W. R. L. Lambrecht and M. van Schilfgaarde, Quasiparticle self-consistent GW calculations of the electronic band structure of bulk and monolayer V_2O_5, *Phys. Rev. B: Condens. Matter Mater. Phys.*, 2015, **91**, 125116.
45 L. R. De Jesus, G. A. Horrocks, Y. Liang, A. Parija, C. Jaye, L. Wangoh, J. Wang, D. A. Fischer, L. F. J. Piper, D. Prendergast and S. Banerjee, Mapping polaronic states and lithiation gradients in individual V_2O_5 nanowires, *Nat. Commun.*, 2016, **7**, 12022.
46 R. Baddour-Hadjean, J. P. Pereira-Ramos, C. Navone and M. Smirnov, Raman microspectrometry study of electrochemical lithium intercalation into sputtered crystalline V_2O_5 thin films, *Chem. Mater.*, 2008, **20**, 1916.
47 R. Baddour-Hadjean and J. P. Pereira-Ramos, Raman microspectrometry applied to the study of electrode materials for lithium batteries, *Chem. Rev.*, 2010, **110**, 1278.
48 D. Huo, A. Contreras, B. Laïk, P. Bonnet, K. Guérin, D. Muller-Bouvet, C. Cenac-Morthe, R. Baddour-Hadjean and J. P. Pereira-Ramos, Evidence for a nanosize effect on the structural and high performance electrochemical properties of V_2O_5 obtained *via* fluorine chemistry, *Electrochim. Acta*, 2017, **245**, 350.
49 H. Jung, K. Gerasopoulos, A. A. Talin and R. Ghodssi, A platform for *in situ* Raman and stress characterizations of V_2O_5 cathode using MEMS device, *Electrochim. Acta*, 2017, **242**, 227.
50 C. V. Ramana, R. J. Smith, O. M. Hussain, M. Massot and C. M. Julien, Surface analysis of pulsed laser-deposited V_2O_5 thin films and their lithium intercalated products studied by Raman spectroscopy, *Surf. Interface Anal.*, 2005, **37**, 406.
51 R. Baddour-Hadjean, V. Golabkan, J. P. Pereira-Ramos, A. Mantoux and D. Lincot, A Raman study of the lithium insertion process in vanadium pentoxide thin films deposited by atomic layer deposition, *J. Raman Spectrosc.*, 2002, **33**, 631.
52 C. Bhandari and W. R. L. Lambrecht, Phonons and related spectra in bulk and monolayer V_2O_5, *Phys. Rev. B: Condens. Matter Mater. Phys.*, 2014, **89**, 045109.

